An Effective Rate Approach to Modeling Single-Stage Spray Drying

Oluwafemi Ayodele George and Xiao Dong Chen
Suzhou Key Laboratory of Green Chemical Engineering, School of Chemical and Environmental Engineering, College of Chemistry, Chemical Engineering and Materials Science, Soochow University, Jiangsu 215123, P.R. China

Dept. of Chemical and Biochemical Engineering, College of Chemistry and Chemical Engineering, Xiamen University, Xiamen 361005, P.R. China

Jie Xiao
Suzhou Key Laboratory of Green Chemical Engineering, School of Chemical and Environmental Engineering, College of Chemistry, Chemical Engineering and Materials Science, Soochow University, Jiangsu 215123, P.R. China

Mengwai Woo
Dept. of Chemical Engineering, Faculty of Engineering, Monash University, Clayton Campus, Melbourne, Victoria 3800, Australia

Liming Che
Dept. of Chemical and Biochemical Engineering, College of Chemistry and Chemical Engineering, Xiamen University, Xiamen 361005, P.R. China

DOI 10.1002/aic.14940
Published online July 18, 2015 in Wiley Online Library (wileyonlinelibrary.com)

An effective rate approach (ERA) is proposed to achieve a fast and reliable prediction of dryer outlet conditions for a given single-stage spray drying system operated under a range of scenarios. This approach is improved from existing methods based on simple mass and energy balances due to the incorporation of a reliable drying rate model, which is the reaction engineering approach for the material of interest. It allows quick solution procedure without the need to solve the partial differential equations that govern the heat and mass transfer in the spray drying process. By following a generic procedure, this technique has been exercised on the experimental results from running a monodisperse droplet spray dryer, that is, a well-established experimental platform for model validation. The proposed ERA has been shown to be rather promising. It could become a powerful approach for proactive control and optimization for existing spray drying facilities. © 2015 American Institute of Chemical Engineers *AIChE J*, 61: 4140–4151, 2015
Keywords: spray drying, predictive modeling, effective rate approach, reaction engineering approach, proactive quality control

Introduction

Spray drying is an effective process for large-scale powder production. Although this technique has been widely used in a variety of industries for many years, proactive control of powder product formation remains a challenge.[1–5] It is well known that the dryer inlet conditions that include the feed solution composition and operational settings all have significant influences on droplet formation through atomization, the air-droplet flow pattern, the air-droplet mass, and heat exchange in the drying chamber, and hence the dryer outlet conditions (i.e., the size, shape, moisture content, and morphology of the particles).[6,7] The quantitative relationships between dryer inlet and outlet conditions, however, remain unclear.

Over the past decades, new dryer designs and optimized operations have been pursued by many research groups to deepen our scientific understanding of the spray drying process and to improve our control over powder formation dynamics. Counter-current spray drying towers are suitable for thermally stable products such as detergents and ceramics as the hot gas comes in contact with dry particles just before the particles exit the tower. Cocurrent spray dryers are the best choice for heat sensitive products like milk powders, where thermal degradation and aroma retention are of concern. Hot gas comes in contact with the droplets at the top where the droplets have maximum moisture content and are at the wet bulb temperature.[8,9] With this configuration, the driest particles are eventually coupled with the lowest temperatures

Correspondence concerning this article should be addressed to J. Xiao at jie.xiao@suda.edu.cn or X. D. Chen at xdc@xmu.edu.cn; xdchen@suda.edu.cn.

(i.e., the outlet temperatures). A single-stream monodisperse droplet spray dryer has been used recently by Rogers et al., Woo et al., Wu et al., and You Xiang[10–17] to investigate the spray drying phenomena. This special set-up gives a better controlled spray drying operation so the experimental data are more useful to validate a range of spray drying models.

Modeling and simulation are effective techniques that provide insights into various spray drying systems and could lead to powerful tools for prediction, control, and optimization. Spray drying process is typically modeled following two contrasting extremes. In the most simplistic manner, the modeling typically follows a "black-box" approach in which the powder coming out from the system is assumed to be completely dried.[9,18] These methods are based on simple mass and energy balances, which can hardly offer comprehensive and reliable predictions. The other extreme is to use advanced fluid flow modeling which captures very detailed phenomena in the process at the expense of time and resources required for computer simulation. Hence, before a decision is reached as to which approach to select for a particular modeling operation, the required level of flexibility, time frame or validity goal, available resources, and the number of approximations that is acceptable, have to be considered.[9]

Note that a comprehensive mathematical model of spray drying operation is very difficult to obtain as a result of high complexity of the physical, chemical, and mechanical properties of such a system. These include for instance, not only the heat and mass transfer within the particle at the boundary between the solid phase and liquid phase but also that between the particle and surroundings. Another important aspect of this complex process is the accounting for the various entrances of the drying medium into the spray dryer and the resulting flow patterns for the gas and the particles.[9] In literature, a significant number of efforts have been reported to characterize the spray drying process using numerical methods, for examples Ali et al.;[8] Jin and Chen;[19–21] Mezhericher et al.;[22] Patel et al.;[7,18] Straatsma et al.;[23] Wang and Langrish;[6] Zbiciński[24]. Wall deposition, agglomeration, powder quality degradation, and so forth, have commonly been studied using Computational Fluid Dynamics (CFD) package ANSYS FLUENT or a version of CFX for both lab or pilot, and industrial-scale spray dryers.[19–21,25–27] These modeling methods all involve considerable iterations which may or may not lead to stable results, and hence can be hardly adopted for proactive process control and system optimization.

In the review work published by Langrish,[28] he categorized well-mixed dryers into coarsest scale modeling. In realizing his approach, he made some assumptions that the outlet gas and the outlet particles being virtually in equilibrium with each other, so that the gas and solids outlet temperatures are almost equal. Neglecting energy losses from the dryer and also assuming that the outlet solids moisture content to be in equilibrium with the gas humidity and gas, he was able to obtain simple expressions for energy and mass balances. While this technique might be suitable for some specific dryer heights and operations, it cannot universally describe mass and energy balancing procedures for spray drying systems.

In summary, spray drying operation is the prime powder production route from liquid. It consumes huge amount of energy. It is desirable to have a powerful strategy for implementing process control and optimization. Model-based predictive control and optimization has not succeeded in industry although it is expected to have great potential. One of the major reasons is that there is hardly a simple and easy way to characterize a complex system with a model that is fast enough to be used online and can represent accurately the drying process. In other words, modeling of spray drying is complex and the models employed have been too time-consuming for online predictive control purposes. Therefore, considerable efforts have been spent recently on a mid-path: finding models and methods that can be worked out with fundamental parameters rather quickly yet they have sufficient fundamental meaning to predict the process well. This is a significantly challenging task. This work is an important attempt to develop a special predictive methodology called as the effective rate approach (ERA) based on the concept of "effective rates." Different from the commonly used black box approaches including the artificial intelligence, neural network approach and genetic algorithms,[29,30] this novel method incorporates a reliable first principle drying rate model (i.e., reaction engineering approach, REA) and allows quick solution derivation without the need to solve drying-kinetics-relevant PDEs.

Effective Rate Approach

An effective rate approach (ERA) is introduced in this section to predict the outlet conditions for a given spray drying system operated under a range of scenarios.

ERA model derivation

A set of partial differential equations (PDEs) that govern the dynamic drying process should be developed. For a one-dimensional (1-D) drying process, these PDEs can be simplified as a set of ordinary differential equations (ODEs).[7,18] Mathematically, this 1-D model can be written as a set of coupled ODEs in a general format

$$\begin{cases} \dfrac{dx_1}{dt}=f_1 \\ \dfrac{dx_2}{dt}=f_2 \\ \vdots \\ \dfrac{dx_i}{dt}=f_i \\ \vdots \\ \dfrac{dx_N}{dt}=f_N \end{cases} \tag{1}$$

where x_1, x_2,. . ., and x_N are key variables defining a spray drying process in a particular spray dryer. In the case study of this work, for instance, six variables are respectively the particle moisture content, particle temperature, air temperature, particle velocity, air humidity, and dryer height.

This model can be numerically solved using some iterative methods, such as the classical Runge–Kutta method, once the initial conditions listed in Eq. 2 are given

$$\begin{cases} x_1(t_0)=x_1^* \\ x_2(t_0)=x_2^* \\ \vdots \\ x_i(t_0)=x_i^* \\ \vdots \\ x_N(t_0)=x_N^* \end{cases} \tag{2}$$

Although detailed process dynamics throughout the drying process (i.e., $x_i(t)$, $t \in [t_0, t_e]$) can be generated, numerous iterations need to be involved before getting the outlet conditions at the time instant t_e.

Instead of solving an ODE set, we propose to use a set of coupled algebraic equations to quantify the outlet conditions, that is

$$x_i(t_e) = x_i^* + \bar{f}_i \times (t_e - t_0) \quad i = 1,\ 2, \ldots, N \tag{3}$$

where $\bar{f}_i$ is the *effective rate* of evolution of the ith variable x_i. Determination of the effective rates under different operating conditions becomes one key task in ERA. According to Eqs. 1 and 3, the effective rate is actually a mean rate, that is

$$\bar{f}_i = \frac{\int_{t_0}^{t_e} f_i dt}{t_e - t_0} \quad i = 1,\ 2, \ldots, N \tag{4}$$

As long as f_i is a continuous function from t_0 to t_e, Eq. 4 can be further written as a weighted mean of the initial and final values of f_i, that is

$$\bar{f}_i = w_i \times f_i(t_0) + (1 - w_i) \times f_i(t_e) \quad i = 1,\ 2, \ldots, N \tag{5}$$

where w_i is the weight, whose value depends on the evolution path of f_i from its initial value to the final value (i.e., the shape of the f_i vs. t curve). Substituting Eq. 5 into Eq. 3 yields the ERA model

$$x_i(t_e) = x_i^* + (w_i \times f_i(t_0) + (1 - w_i) \times f_i(t_e)) \times (t_e - t_0) \quad i = 1,\ 2, \ldots, N \tag{6}$$

with

$$f_i(t_0) = F_i\left(x_1^*, x_2^*, \cdots, x_N^*, t_0\right) \tag{7}$$

$$f_i(t_e) = F_i(x_1(t_e), x_2(t_e), \cdots, x_N(t_e), t_e) \tag{8}$$

where F_i is a known function given in Eq. 1. For a specific spray drying system operated under a specified scenario, the initial conditions (at $t_0 = 0$) are usually given. If the weight w_i can be determined, the outlet conditions at time instant t_e can be readily obtained by solving the ERA model, that is, the coupled algebraic equation set listed in Eq. 6. Compared with the ODE model, the ERA model predicts outlet conditions without the involvement of numerical iterations and hence significantly reduces the computational effort. It should be noted that some ODEs may be solved very fast. However, solving algebraic equation systems as formulated in ERA is much faster. The computational time difference between solving one ODE set and one algebraic equation set may be negligible. In advanced model-based control and optimization, however, using an ODE model or an algebraic model may lead to significant differences in computational efforts. Because one then has to solve a tremendous amount of ODE sets or algebraic equation sets before obtaining an optimal solution.

Effective rate determination

The key for the success of ERA is a reliable value of the effective rate. Specifically, in the current ERA model (i.e., Eq. 6), the weight w_i should be determined rationally. It is understandable that different inlet conditions will lead to different process dynamics, that is, different effective rates. Specifically, initial values of a number of variables in Eq. 6, which include precursor solution compositions and operational settings, simultaneously affect the drying dynamics. In this work, we focus our efforts on the cases where different drying dynamics are caused by the change of initial values of two key variables.

To determine effective rates, we first calculate w_i using Eq. 6 with outlet conditions measured in experiments under prespecified initial conditions. Then, the weights under other conditions can be determined through linear/nonlinear interpolation.

ERA-based calculation procedure

The following procedure can be followed to predict the outlet conditions of a given spray drying system.

Step 1. Develop a 3-D PDE model and simply it to a 1-D ODE model (i.e., Eq. 1) for the spray drying system.

Step 2. Transform the ODE model into the ERA model (i.e., Eq. 6).

Step 3. Identify two key operating variables (i.e., x_j and x_k) as well as feasible ranges of their initial values (i.e., $[x_{j,\min}^*, x_{j,\max}^*]$ and $[x_{k,\min}^*, x_{k,\max}^*]$). These variables can be the ones that are conventionally manipulated to control the outlet conditions.

Step 4. Design a set of representative experiments that can cover the ranges identified in *Step 3*. Each experiment refers to a specific combination of x_j^* and x_k^*, where $x_j^* \in [x_{j,\min}^*, x_{j,\max}^*]$ and $x_k^* \in [x_{k,\min}^*, x_{k,\max}^*]$. For each experiment, measure the outlet conditions (i.e., $\hat{x}_i(\hat{t}_e)$ and $\hat{t}_e$) and obtain w_i by solving Eq. 6.

Step 5. Derive w_i for spray drying cases under any combination of x_j^* and x_k^* using linear/nonlinear interpolation.

Step 6. Predict the outlet conditions using Eq. 6 with the weight values obtained in *Step 5*.

Results and Discussion

A single-stream monodisperse droplet spray dryer was investigated in this section to demonstrate the efficacy of the general ERA method in outlet conditions prediction. The advantage here is to make sure the initial droplet size is uniform to eliminate the effect of a wide droplet size distribution which usually detriments the validation of a modeling exercise. By resorting to this pilot scale spray dryer developed by Chen and coworkers,[13,16] uniform-sized droplets experience similar drying history, which allows a definitive study of the influences of different spray drying conditions on the product characteristics. This facility has demonstrated unique potential in validating a set of predictive models (from 1-D to 3-D), which has led to an improved understanding of the spray drying system.[19–21,28,31–33]

Process description and system specification

Three basic steps are usually involved in a spray drying process: the atomization of the feed into a spray of fine droplets, the evaporation of droplets by a stream of heated gas and finally, the separation of the dried powder from the gas stream at the dryer exit. For the monodisperse droplet spray dryer investigated in this work, a schematic of its main drying chamber is given in Figure 1.

Any liquid feed entering the dryer is first atomized using a microfluidic nozzle into single streams of fine droplets. Hot air is introduced with variable temperature heat guns at the top of drying chamber. An air dispersion plate with small holes is utilized to evenly distribute the airflow throughout the column. The total mass flow rate of air going into the chamber is 8.98×10^{-3} kg s^{-1}, making it about 538:1 relative to the liquid flow rate. Key variables defining this spray drying process include the particle moisture

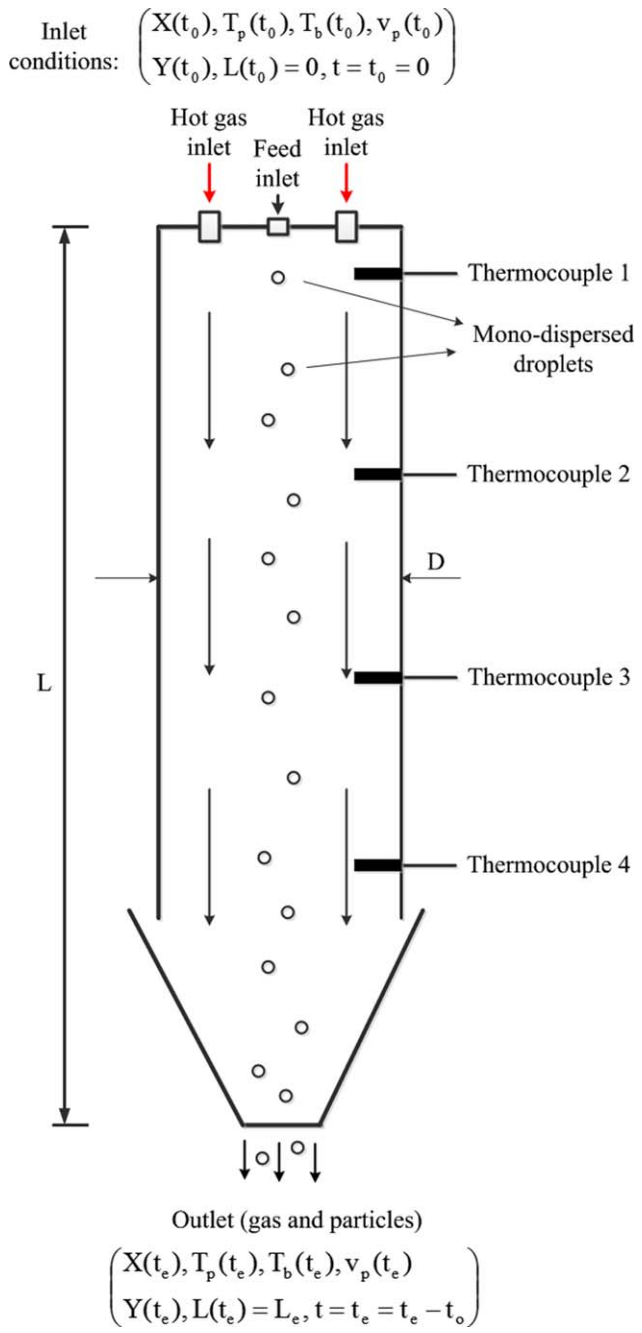

Figure 1. Schematic of the monodisperse spray dryer.

[Color figure can be viewed in the online issue, which is available at wileyonlinelibrary.com.]

content, particle temperature, air temperature, particle velocity, air humidity, and dryer height (see Figure 1). Their initial values for a skim milk drying process are listed in Table 1.

Inside the dryer, flying droplets interact with the hot air through simultaneous exchange of momentum, energy, and mass, which causes rapid surface evaporation. Toward the lower part of the dryer, where the temperature is relatively low, evaporation slows down and becomes limited by diffusion of liquid from the center to the surface of a droplet. For this reason, it is always preferable to spray dry heat sensitive products using the concurrent configuration as shown in Figure 1.

At the outlet, most particles reach equilibrium, so their moisture contents are limited by the equilibrium moisture content given by the Guggenheim–Anderson–deBoer (GAB) model. For a well conserved system, mass and energy losses are usually neglected. This particular spray dryer is insulated with a fiberglass lagging system, so overall heat loss coefficient across the dryer is limited to approximately 1.5 J s^{-1} m^{-2} K^{-1}. It is a critical parameter to determine the air temperature and particle temperature at the outlet.

ERA model implementation

ODE Model Development (Step 1). Most spray drying models exist as 3-D partial differential equations (PDEs).[5–7] A 1-D model has been established previously for the monodisperse droplet spray dryer.[7,18] In model development, the spray dryer was treated as a 1-D plug-flow reactor having a cocurrent flow and all the spherical-shaped droplets in the dryer at the same altitude were assumed to have identical properties. Here, we briefly summarize the 1-D model (i.e., a set of ordinary differential equations). Readers can refer to our previous papers for detailed derivations.[8,10,12,18] All variables together with their units are listed in the Notation section. The critical part of this model is the Reaction Engineering Approach (REA) that describes the drying kinetics

$$\frac{dX}{dt} = -\frac{h_m A_p \left[\rho_{v,\mathrm{sat}} \exp\left(-\frac{\Delta E_v}{R_g T_p}\right) - \rho_{v,b}\right]}{m_s} = f_1 \tag{9}$$

A brief description of REA has been given in the Appendix. The droplet/particle temperature and the bulk temperature dynamics can be obtained based on the energy balance

$$\frac{dT_p}{dt} = -\frac{hA_p(T_b - T_p) - m_s \frac{dX}{dt}\Delta H_L}{m_w C_{p,w} + m_s C_{p,s}} = f_2 \tag{10}$$

$$\frac{dT_b}{dt} = \frac{\left[-m_s \frac{dX}{dt}\theta C_{p,v}(T_b - T_p)\right] - \theta h A_p (T_b - T_p) - U v_p (\pi D)(T_b - T_{\mathrm{amb}})}{\dot{m} C_{p,b}} = f_3 \tag{11}$$

Rearranging the equation of motion results in the equation for droplet/particle velocity evolution

$$\frac{dv_p}{dt} = \frac{C_D 18 \mu_b R_e (v_b - v_p)}{24 \rho_p d_p^2} + \frac{g}{\rho_p}(\rho_p - \rho_b) = f_4 \tag{12}$$

where d_p is the droplet diameter, which evolves over time as well. It has been experimentally validated that skim milk droplet shrinkage follows a linear shrinkage behavior, that is, a linear relationship between the droplet size and its moisture content.[18,34] Moisture removal from the droplet leads to the change of the bulk air humidity

$$\frac{dY}{dt} = \frac{\theta m_s \frac{dX}{dt}}{\dot{m}_{b,\mathrm{dry}}} = f_5 \tag{13}$$

The distance traveled by a droplet can be correlated with its velocity by

$$\frac{dL}{dt} = v_p = f_6 \tag{14}$$

The 1-D drying model to be solved consists of Eqs. 9–14 with initial conditions specified below

Table 1. Inlet Conditions for Skim Milk Drying Using the Monodisperse Spray Dryer

Feed/Gas Parameters							
Inlet Gas Conditions							
T_b^* (°C)	183	165	157	149	135	111	90
Y^* (kg water kg^{-1}, db)	0.0078	0.0078	0.0078	0.0078	0.0078	0.0078	0.0078
Flow rate (kg h^{-1})	32.33	32.33	32.33	32.33	32.33	32.33	32.33
Inlet Skim Milk Conditions							
T_p^* (°C)	20	20	20	20	20	20	20
Initial solid concentration (%)	20	20	20	20	20	20	20
X^* (kg kg^{-1}, db)	4	4	4	4	4	4	4
v_p^* (m s^{-1})	3.53	3.53	3.53	3.53	3.53	3.53	3.53
Flow rate (kg h^{-1})	0.06	0.06	0.06	0.06	0.06	0.06	0.06
Droplet initial diameter (μm)	190	190	190	190	190	190	190
	200	200	200	200	200	200	200
	210	210	210	210	210	210	210

$$\begin{cases} X(t_0)=X^* \\ T_p(t_0)=T_p^* \\ T_b(t_0)=T_b^* \\ v_p(t_0)=v_p^* \\ Y(t_0)=Y^* \\ L(t_0)=L^*=0 \end{cases} \tag{15}$$

Note that initial values for six independent variables (i.e., dryer inlet conditions) have been specified in the system specification part (see Table 1). The distance traveled by a droplet at the beginning of the process is obviously zero.

ERA Model Development (Step 2). One can then readily transform the ODE model into the ERA model based on Eq. 6. The algebraic equation set for outlet conditions is listed below

$$\begin{cases} X(t_e)=X^*+(w_1\times f_1(t_0)+(1-w_1)\times f_1(t_e))\times(t_e-t_0) \\ T_p(t_e)=T_p^*+(w_2\times f_2(t_0)+(1-w_2)\times f_2(t_e))\times(t_e-t_0) \\ T_b(t_e)=T_b^*+(w_3\times f_3(t_0)+(1-w_3)\times f_3(t_e))\times(t_e-t_0) \\ v_p(t_e)=v_p^*+(w_4\times f_4(t_0)+(1-w_4)\times f_4(t_e))\times(t_e-t_0) \\ Y(t_e)=Y^*+(w_5\times f_5(t_0)+(1-w_5)\times f_5(t_e))\times(t_e-t_0) \\ L(t_e)=(w_6\times f_6(t_0)+(1-w_6)\times f_6(t_e))\times(t_e-t_0) \end{cases} \tag{16}$$

where t_e-t_0 gives the particle residence time and the initial time instant t_0 is conventionally set to 0. The mathematical expressions for f_1 to f_6 have been listed in Eqs. 9–14. At the dryer outlet, the distance traveled by a particle equals to the height of the tower (i.e., $L(t_e) = L_e$).

Key Variable Identification (Step 3). Our monodisperse spray dryer is equipped with different spray nozzles to generate different sized droplets from a variety of precursor solutions. One conventionally manipulated operating condition is the inlet air temperature, which allows droplets to experience different drying histories. Thus, the selected representative variables are the initial droplet size (d_p^*) and the inlet air temperature (T_b^*). In this study, the initial droplet diameter ranges from 190 μm to 210 μm and the inlet air temperature can be controlled at a value between 90°C to 220°C.

Effective Rate Determination (Step 4 and Step 5). As stated in the methodology part, a critical step toward a reliable ERA model is the derivation of effective rates, which are determined by the weights (w_1 to w_6) listed in Eq. 16. Their values can be obtained by solving the algebraic equation set (i.e., Eq. 16) as long as the outlet conditions and the residence time are given.

Since different inlet conditions will lead to different drying kinetics and hence different effective rates, we need to derive the values of weight parameters for any specific combination of d_p^* and T_b^*, where $d_p^* \in [190\ \mu\text{m}, 210\ \mu\text{m}]$ and $T_b^* \in [90°\text{C}, 220°\text{C}]$. The idea is first to get weight values for selected experimental conditions based on measurement data of outlet conditions and the residence time, and then to derive weight values for other conditions through interpolation. A set of representative experiments should be designed that can cover the ranges of d_p^* and T_b^*. In this work, nine individual *in silico* experiments (i.e., the three by three design in Table 2) were carried out using the validated 1-D drying model (i.e., Eqs. 9–15). Solving the ODE set with the dryer height and initial conditions listed in Table 1, one can readily obtain the outlet

Table 2. Three by Three Design of *In Silico* Experiments

Initial Droplet Diameter (μm)	Air Inlet Temperature (°C)	Parameter[a]					
		w_1	w_2	w_3	w_4	w_5	w_6
190	120	0.426835	0.022932	0.048000	0.005602	0.427337	0.018238
	165	0.349458	0.030225	0.011235	0.005336	0.349873	0.013238
	220	0.276987	0.034816	−0.022699	0.005082	0.277315	0.010921
200	120	0.492606	0.021631	0.054394	0.006705	0.493177	0.024374
	165	0.420030	0.030973	0.031221	0.006347	0.420530	0.016022
	220	0.334063	0.038222	−0.009635	0.006064	0.334459	0.013191
210	120	0.552512	0.018759	0.061295	0.007925	0.553146	0.031707
	165	0.498928	0.030818	0.052929	0.007476	0.499520	0.019342
	220	0.399323	0.040353	0.007159	0.007168	0.399798	0.015698

[a]Values for weighted parameters were obtained by solving the ERA model (i.e., Eq. 16).

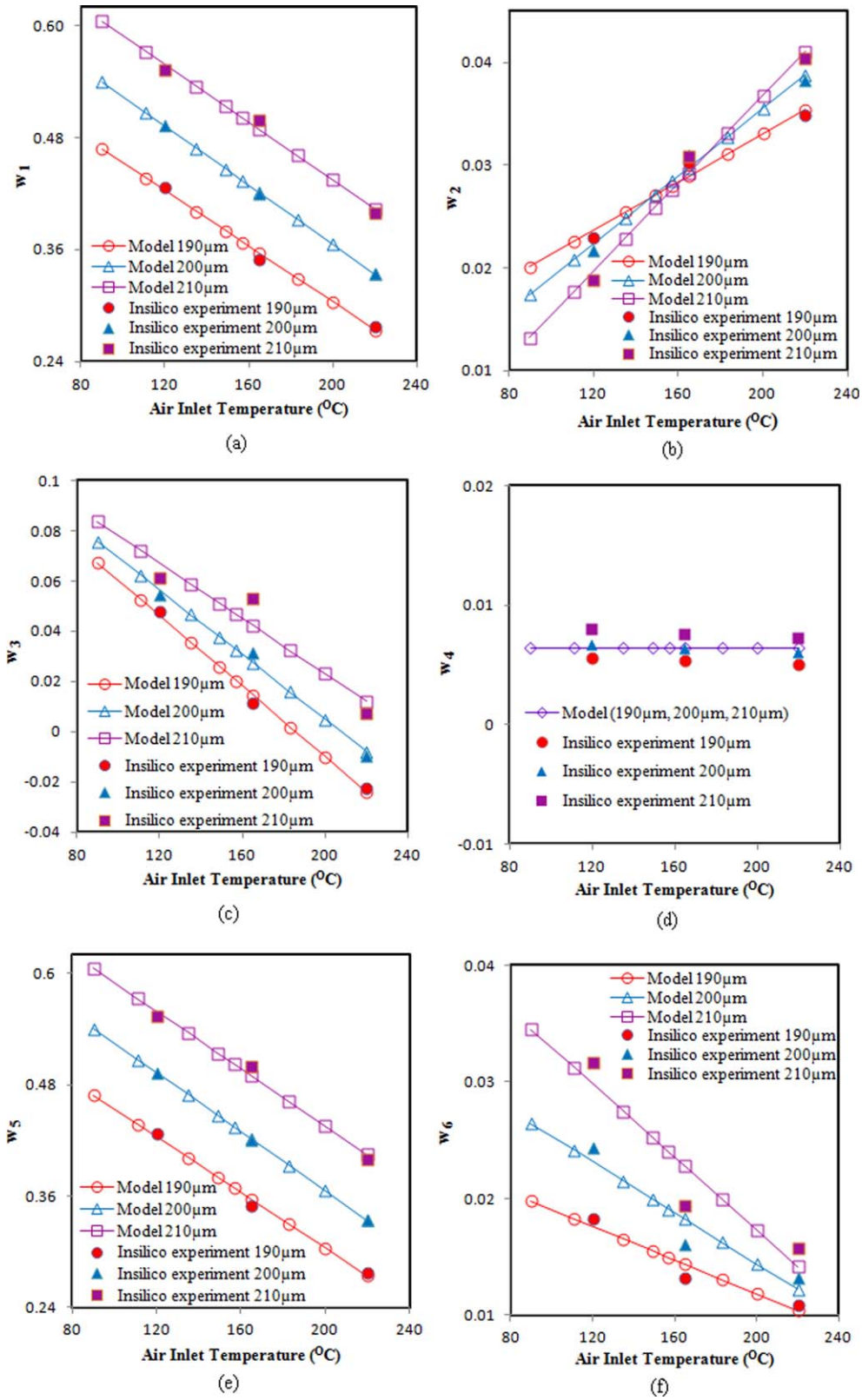

Figure 2. Profiles of weighted parameters as a function of air inlet temperature and initial droplet diameter.

(a), (b), (c), (d), (e), and (f) represent weights w_1, w_2, w_3, w_4, w_5, and w_6, respectively. [Color figure can be viewed in the online issue, which is available at wileyonlinelibrary.com.]

conditions $\left(\hat{X}(\hat{t}_e), \hat{T}_p(\hat{t}_e), \hat{T}_b(\hat{t}_e), \hat{v}_p(\hat{t}_e), \hat{Y}(\hat{t}_e)\right)$ and the residence time $(\hat{t}_e)$ for each experiment. Plugging these data into Eq. 16 and solving the algebraic equation set, we get the values of weight parameters (w_1, w_2, w_3, w_4, w_5, w_6), which are listed in Table 2 and plotted as filled shapes in Figure 2. For each initial droplet diameter, linear relationships can be identified between weight parameters and inlet temperatures (see straight lines and hollow shapes in Figure 2). Since the range

Table 3. Values of Weighted Parameters Obtained Using Linear Interpolation

Initial Droplet Diameter (μm)	Air inlet Temperature (°C)	Parameter					
		w_1	w_2	w_3	w_5	w_6	w_4
		Linear Relationship					Constant Average
190	90	0.467957	0.020117	0.067301	0.468508	0.019775	0.006412
	111	0.436628	0.022585	0.052524	0.437142	0.018262	
	135	0.400823	0.025407	0.035635	0.401295	0.016534	
	149	0.379937	0.027052	0.025784	0.380385	0.015525	
	157	0.368002	0.027993	0.020154	0.368436	0.014949	
	165	0.356067	0.028933	0.014525	0.356487	0.014373	
	183	0.329213	0.031049	0.001858	0.329602	0.013076	
	200	0.303851	0.033047	−0.010104	0.304210	0.011852	
	220	0.274014	0.035398	−0.024178	0.274338	0.010411	
200	90	0.539694	0.017377	0.075776	0.540321	0.026450	
	111	0.506417	0.020835	0.062251	0.507008	0.024148	
	135	0.468387	0.024787	0.046795	0.468935	0.021517	
	149	0.446202	0.027092	0.037778	0.446726	0.019982	
	157	0.433525	0.028409	0.032626	0.434035	0.019105	
	165	0.420848	0.029727	0.027474	0.421344	0.018228	
	183	0.392325	0.032691	0.015881	0.392790	0.016255	
	200	0.365387	0.035490	0.004933	0.365821	0.014392	
	220	0.333695	0.038783	−0.007948	0.334094	0.012199	
210	90	0.604385	0.013184	0.083700	0.605077	0.034521	
	111	0.572001	0.017686	0.072108	0.572659	0.031231	
	135	0.534991	0.022831	0.058861	0.535611	0.027471	
	149	0.513402	0.025832	0.051133	0.513999	0.025278	
	157	0.501065	0.027547	0.046717	0.501649	0.024024	
	165	0.488728	0.029262	0.042301	0.489300	0.022771	
	183	0.460971	0.033121	0.032366	0.461513	0.019951	
	200	0.434755	0.036766	0.022982	0.435270	0.017288	
	220	0.403913	0.041053	0.011943	0.404396	0.014155	

of values from experimental trials for w_4 is significantly smaller than those for w_1, w_2, w_3, w_5, and w_6, we, therefore, adopted a constant average for w_4 (Figure 2d).

ERA Model Prediction (Step 6). 0.02w?>Using the identified weight values listed in Table 3, Eq. 16 can be solved to generate outlet conditions under specified inlet conditions. Figures 3 and 4 show the final moisture content, particle and air temperatures, particle velocity, air humidity, and particle residence time as a function of the inlet air temperature, and the initial droplet diameter. ERA produced predictions which were well correlated with experimental measurements for final moisture content only at one click (see Figure 3). As shown in Figure 3, the trends identified from experimental data have been successfully reproduced by the ERA model. When the initial droplet size is specified, increasing the inlet air temperature can lead to a decrease of the particle's final moisture content. With the same inlet air temperature, decreasing the initial droplet size leads to lower particle moisture content. Also note that it is extremely difficult to precisely control and measure the initial droplet size in experiments. The predictions shown in Figure 3 should be satisfactory considering the uncertainties in experimental results. Actually, the prediction precision of the current ERA model is not lower than that of a comprehensive CFD model (see CFD results in Yang et al., 2015).[31]

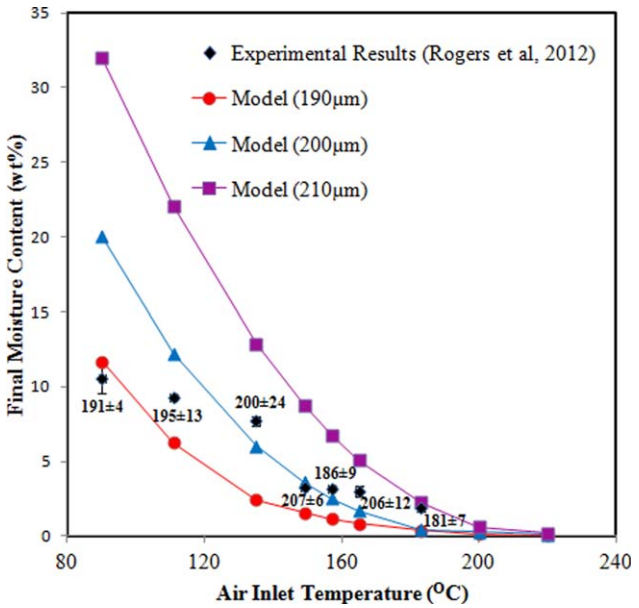

Figure 3. Particle final moisture content for different air inlet temperatures and initial droplet diameters compared with experimental measurements.

Initial droplet diameters used in the experiments are shown with the labels. [Color figure can be viewed in the online issue, which is available at wileyonlinelibrary.com.]

Discussion

Effective rate approach is undoubtedly a promising technique for industrial-wide spray drying operations when a quick assessment of the outlet conditions is desired. In this study, the input temperature ranges from 90°C to 220°C while initial droplet diameter varies within 190–210 μm, which is a representation of typical ranges of spray drying operational settings. Different initial conditions such as air and particle temperature, air and feed flow rate, droplet size, and solid concentration, all have varying outcomes on the outlet state of particles.[35–38] Figures 3 and 4 show effects of air inlet temperature and initial droplet size variations on the outlet particle conditions predicted by our model.

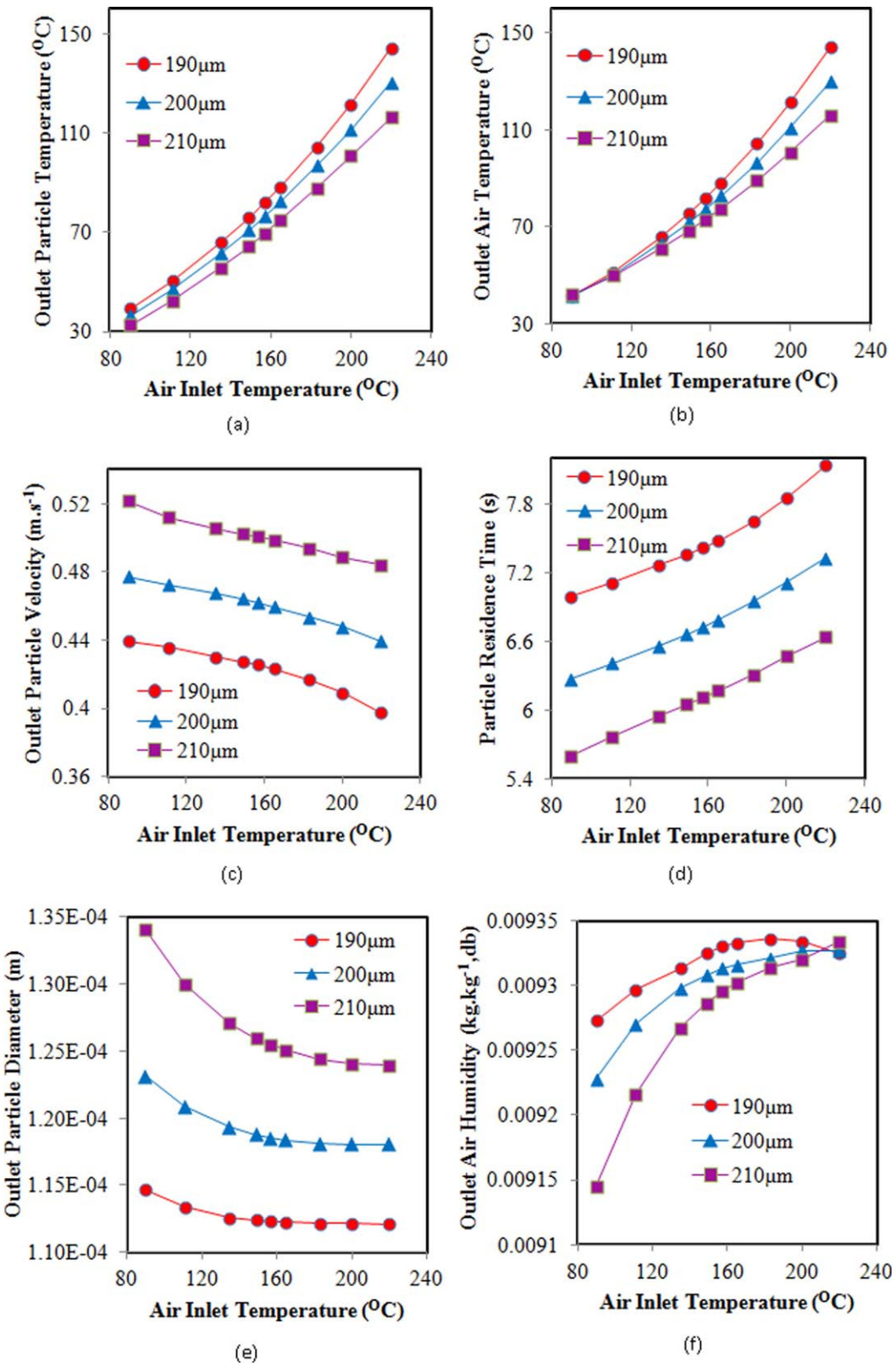

Figure 4. Profiles of outlet conditions for different inlet air temperatures and initial droplet diameters: (a) outlet particle temperature, (b) outlet air temperature, (c) particle outlet velocity, (d) particle residence time profiles, (e) outlet particle diameter, and (f) outlet air humidity.

[Color figure can be viewed in the online issue, which is available at wileyonlinelibrary.com.]

Effects of Air Inlet Temperature. As shown in Figures 3 and 4, the inlet air temperature ranges from 90°C to 220°C with different corresponding particle outlet conditions. For each run of air inlet temperature, the outlet particle and air temperatures varied from 39°C to 144°C and 49°C to 144°C respectively for droplets with an initial size of 190 μm (Figures

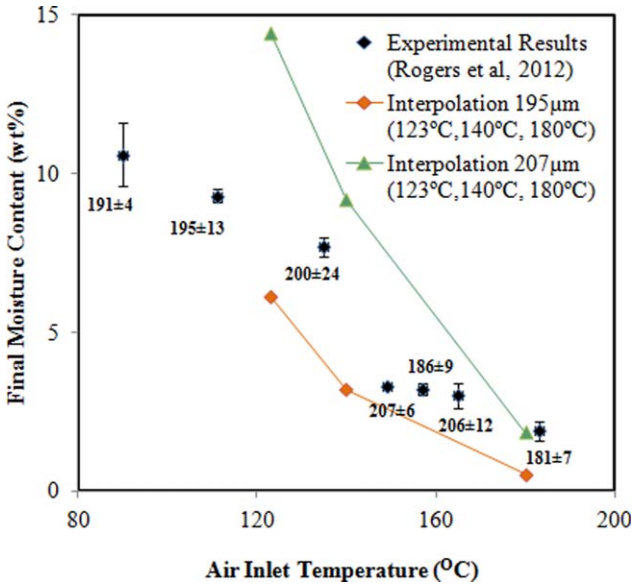

Figure 5. Final moisture content profiles of particles spray dried under randomly selected combinations of air inlet temperatures and initial droplet diameters.

[Color figure can be viewed in the online issue, which is available at wileyonlinelibrary.com.]

4a, b), similar to the range of skim milk powder results obtained by Oldfield, et al.[35]

According to Figure 3, temperature shows a significant influence on the powder moisture content (e.g., 0.06–11.67wt % for 190 μm droplets). This is due to the fact that, at higher air inlet temperatures, there is a greater temperature gradient between the atomized feed and the drying air, resulting in a greater driving force for water evaporation and thus producing powders with lower moisture content.[39] In addition, an increase in air inlet temperature is accompanied by a proportional increase in enthalpy air input. As a consequence, the amount of heat received by the droplet is also raised, its outlet temperature is higher and the final moisture content is reduced (Figures 3 and 4a).

Furthermore, higher air inlet temperatures gave rise to lower outlet particle velocity and higher residence time for droplets of the same size (Figures 4c, d). This is because drying at higher temperatures leads to smaller particles with less moisture contents (see Figures 3 and 4e). Smaller particles tend to have lower velocities. For a given distance traveled by the droplet, an inverse relationship exists between the droplet velocity and residence time according to Eq. 14. So, an increase in residence time is always prompted by a decrease in velocity.

For the case with 190 μm droplets, the outlet air humidity rose sequentially from 0.009273 kg/(kg, db) at 90°C, then declined from 0.009334 kg/(kg, db) to 0.009325 kg/(kg, db) between 200°C and 220°C (see Figure 4f). It is believed that at higher air inlet temperatures (characterized by longer residence time), rewetting of particles could take place. This phenomenon may affect particle structure, and it is of interest to quality control in spray drying.[31]

Effects of Initial Droplet Size. Monodisperse spray dryer provides us with unique opportunities to explore the effects of initial droplet size on product formation during spray drying. The shrinkage of a milk droplet follows a linear model, which is a function of the droplet moisture content (see Eq. A6). The different sized droplets in this study, although with the same initial solid concentration, experienced different shrinkage behaviors across the temperature range from 90°C to 220°C (see the different curves of final moisture content in Figure 3). The Guggenheim–Anderson–deBoer (GAB) model, which has been fitted at elevated temperatures (up to 90°C) and a wide range of relative humidity (up to 100%), was used to calculate equilibrium moisture content of milk droplets (Eq. A17). Particles exiting the dryers are expected to have reached their equilibrium moisture content as given by the desorption isotherm. Furthermore, during the course of drying, a droplet usually experiences drag force opposing its flight. The magnitude of drag experienced by a droplet depends on the droplet size, shape, speed, and the properties of the fluid, which have coupled effects on the final product properties.

As shown in Figure 4, smaller droplets with identical shrinkage behavior stayed longer in the chamber, thereby experiencing longer drying time. For a situation where the initial droplet size is reduced, its total surface area and velocity are reduced. A reduction in the droplet's Reynolds number causes the force opposing its motion to be more pronounced, leading to lesser speed (Figure 4c). This results in extended mass transfer action because the droplet's residence time is prolonged (Figure 4d). Denaturation of proteins in milk droplets has been linked to high temperatures. In other words, larger droplets generally favor generation of low particle temperature in the dryer (Figure 4a).

Further Remarks. By interpolating within the temperature-diameter graphs, respective values of the weighted parameters can be obtained for other input conditions desired. Further analyses on particle formation were carried out by interpolating for two different initial droplet diameters (i.e., 195 μm and 207 μm) spray dried using three interpolated air inlet temperatures 123°C, 140°C, and 180°C respectively. As expected, prediction results show consistent trend of outlet particle moisture contents (Figure 5), which are comparable with experimental results. Similar findings were also obtained for other outlet conditions (results not shown) such as air and particle outlet temperatures, outlet air humidity, residence time, and outlet particle velocity, indicating the effectiveness of ERA model in providing consistent results.

In this study, we selected two key operating variables, that is, air inlet temperature and initial droplet diameter, necessary to control and optimize industrial spray dryers for real time scenarios. These two are of course very important two. It should be pointed out that the generic ERA method is not restricted to predicting dryer outlet conditions under different combinations of inlet air temperature and inlet droplet diameter. If necessary, other operating variables such as the air flow rate, liquid feed flow rate, inlet solid concentration and temperature of droplets can be selected as well. As long as only one or a pair of inlet conditions is manipulated simultaneously, the same procedure can be followed to uniquely identify the values of weight parameters from a plot similar to Figure 2. Hence, effective rates and outlet conditions can be uniquely determined using Eq. 16. In most cases, it is sufficient to manipulate two key variables simultaneously for the control and optimization of a spray drying process. How to uniquely identify effective rates when more than two operating variables are involved simultaneously will be addressed in our future study.

Conclusions

An effective rate approach (ERA) to a single-stage spray drying modeling has been proposed and developed in this work. This method enables a fast estimation of the dryer outlet parameters such as humidity, moisture content, temperature, velocity, and residence time. The key idea is to simplify the partial differential equation set that governs the dynamic drying process into a set of algebraic equations using the concept of "effective rates," so that the time-consuming iterative numerical scheme for solving PDEs/ODEs can be avoided. A general procedure has been outlined to implement the ERA and ensure the effective rates to reflect the droplet drying dynamics in a spray dryer operated under different conditions. Necessary equations and solutions were developed which have been discussed accordingly.

The ERA method requires a drying kinetics model of single droplet drying of the liquid of concern, such as a REA model, to be known prior. This is known to be reliable and easy to obtain for the model parameters. This approach has been validated using the experimental data from running a monodisperse droplet spray dryer. The advantage of this dryer is that the inlet condition of the spray in terms of the initial droplet diameter and location can be accurately defined, which is not possible in other spray drying devices. The predictions are with respects to changing inlet conditions for air temperature and inlet droplet diameter for the same kind of material, that is, 20 wt % skim milk in this work. The estimated outlet moisture contents are found to satisfactorily match experimental measurements. Detailed analyses have further confirmed that the process is highly influenced by the inlet conditions, which has been successfully captured by ERA. More comprehensive and detailed experiments will be carried out in future work to test the effectiveness of the ERA concept for industrial-scale poly-dispersed spray drying systems. Nevertheless this work has provided a generic framework, by following which outlet conditions of a spray dryer could be predicted timely on a desktop computer. The ERA could become a promising tool for process control and optimization.

Notation

w_1, w_2, w_3, w_4, w_5, w_6 = weights in the ERA model
v_p = particle or droplet velocity, m s^{-1}
$t_e - t_0$ = residence time, s
d_p = particle or droplet diameter, m
g = gravitational acceleration, m s^{-2}
T_b = air temperature, K
T_p = particle temperature, K
T_{amb} = ambient Temperature, K
$C_{p,w}$ = specific heat capacity of water, J kg^{-1} K^{-1}
$C_{p,s}$ = specific heat capacity of solid, J kg^{-1} K^{-1}
$C_{p,b}$ = specific heat capacity of bulk air, J kg^{-1} K^{-1}
$\dot{m}_{p,total}$ = total feed mass flow rate, kg s^{-1}
$\dot{m}$ = mass flow rate of bulk air, kg s^{-1}
$\dot{m}_{b,dry}$ = mass flow rate of dry air, kg s^{-1}
ΔH_L = latent heat of water vaporization, J kg^{-1}
Y = bulk air absolute humidity, kg kg^{-1}, db
$\frac{dm_w}{dt}$ = drying rate of a single droplet, kg s^{-1}
A_p = area of particle or droplet, m^2
h = heat-transfer coefficient, J s^{-1} m^{-2} K^{-1}
U = heat loss coefficient, J s^{-1} m^{-2} K^{-1}
D = diameter of the chamber, m
L_e = length or height of the tower, m
h_m = mass-transfer coefficient, m s^{-1}
R_g = universal gas constant, 8.314 J kg^{-1} K^{-1}
ΔE_v = REA activation energy, J kg^{-1}
$\Delta E_{v,b}$ = REA equilibrium activation energy, J kg^{-1}
x_{water} = mass fraction of water, kg kg^{-1}
x_{air} = mass fraction of air, kg kg^{-1}
Mr = molecular weight, kg $kmol^{-1}$
P = pressure, Pa
m_w = mass of water, kg
m_s = mass of solid, kg
P_v = partial pressure of vapor, Pa
X = particle moisture on dry basis, kg kg^{-1}, db
X_b = equilibrium moisture on dry basis, kg kg^{-1}, db

Greek letters

μ = viscosity, kg m^{-1} s^{-1}
ρ_v = vapor density, kg m^{-3}
θ = number of particles or droplets per second

Subscripts and superscripts

* = initial value
b = bulk air
p = particle or droplet
sat = saturated condition

Acknowledgments

We acknowledge the financial supports from Soochow University and Xiamen University (China), "Research and Development of Spray Drying Equipment," 863 Project, National Natural Science Foundation of China (2011AA100801-3 and No. 21406148), Jiangsu Specially-Appointed Professors Program, Jiangsu Innovation and Entrepreneurship (Shuangchuang) Program, the Priority Academic Program Development (PAPD) of Jiangsu Higher Education Institutions, Natural Science Foundation of Jiangsu Province (No. BK20130293), Kingdom Way Ltd (Xiamen), and Monash University (Australia).

Literature Cited

1. Chen XD, Sidhu H, Nelson M. Theoretical probing of the phenomenon of the formation of the outermost surface layer of a multicomponent particle, and the surface chemical composition after the rapid removal of water in spray drying. *Chem Eng Sci*. 2011;66(24):6375–6384.
2. Kawakami K, Sumitani C, Yoshihashi Y, Yonemochi E, Terada K. Investigation of the dynamic process during spray-drying to improve aerodynamic performance of inhalation particles. *Int J Pharm*. 2010;390(2):250–259.
3. Vicente J, Pinto J, Menezes J, Gaspar F. Fundamental analysis of particle formation in spray drying. *Powder Technol*. 2013;247:1–7.
4. Keshani S, Daud WRW, Nourouzi MM, Namvar F, Ghasemi M. Spray drying: an overview on wall deposition, process and modeling. *J Food Eng*. 2015;146:152–162.
5. Reinhard V, Willard RF, David L-B. Particle formation in spray drying. *J Aerosol Sci*. 2007;38:728–746.
6. Wang S, Langrish TAG. A review of process simulations and the use of additives in spray drying. *Food Res Int*. 2009;42(1):13–25.
7. Patel KC, Chen XD. Prediction of spray-dried product quality using two simple drying kinetics model. *J Food Process Eng*. 2005;28:567–594.
8. Ali M, Mahmud T, Heggsa PJ, Ghadiria M, Djurdjevicb D, Ahmadianb H, de Juanb LM, Amadorb C, Baylyb A. A one-dimensional plug-flow model of a counter-current spray drying tower. *Chem Eng Res Des*. 2014;92(5):826–841.
9. Shayantharan S. *Modelling and Control of a Spray Drying Process*. Department of Electrical Engineering, Technical University of Denmark, Denmark, 2009.
10. Rogers S, Fang Y, Qi Lin SX, Selomulya C, Chen XD. A monodisperse spray dryer for milk powder: modelling the formation of insoluble material. *Chem Eng Sci*. 2012;71:75–84.
11. Rogers S, Wu WD, Lin SXQ, Chen XD. *A monodisperse spray dryer for milk powder: investigation of particle shrinkage and puffing*. CHEMECA. Adelaide, Australia 2010:1288–1297.

12. Rogers S, Wu WD, Lin SXQ, Chen XD. Particle shrinkage and morphology of milk powder made with a monodisperse spray dryer. *Biochem Eng J*. 2012;62:92–100.
13. Woo MW, Rogers S, Lin SXQ, Selomulya C, Chen XD. Numerical probing of a low velocity concurrent pilot scale spray drying tower for mono-disperse particle production—unusual characteristics and possible improvements. *Chem Eng Process*. 2011;50(4):417–427.
14. Woo MW, Rogers S, Selomulya C, Chen XD. Particle drying and crystallization characteristics in a low velocity concurrent pilot scale spray drying tower. *Powder Technol*. 2012;223:39–45.
15. Wu W, Amelia R, Hao N, Selomulya C, Zhao D, Chiu Y, Chen XD. Assembly of uniform photoluminescent microcomposites using a novel micro-fluidic-jet-spray-dryer. *AIChE J*. 2011;57(10):2726–2737.
16. Wu WD, Lin SX, Chen XD. Monodisperse droplet formation through a continuous jet break-up using glass nozzles operated with piezoelectric pulsation. *AIChE J*. 2011;57(6):1386–1392.
17. You X. *Dairy Milk Particles Made with a Mono-Disperse Droplet Spray Dryer (MDSD) Investigated for the Effect of Fat*. Department of Chemical and Biochemical Engineering, Xiamen University, Xiamen, China, 2013.
18. Patel K, Chen XD, Jeantet R, Schuck P. One-dimensional simulation of co-current, dairy spray drying systems—pros and cons. *Dairy Sci Technol*. 2010;90(2–3):181–210.
19. Jin Y, Chen XD. A fundamental model of particle deposition incorporated in CFD simulations of an industrial milk spray dryer. *Dry Technol*. 2010;28(8):960–971.
20. Jin Y, Chen XD. Numerical study of the drying process of different sized particles in an industrial-scale spray dryer. *Dry Technol*. 2009; 27(3):371–381.
21. Jin Y, Chen XD. A three-dimensional numerical study of the gas/particle interactions in an industrial-scale spray dryer for milk powder production. *Dry Technol*. 2009;27(10):1018–1027.
22. Mezhericher M, Levy A, Borde I. Spray drying modelling based on advanced droplet drying kinetics. *Chem Eng Process*. 2010;49(11): 1205–1213.
23. Straatsma J, Houwelingen GV, Steenbergen AE, De Jong P. Spray drying of food products: 1. Simulation model. *J Food Eng*. 1999;42: 67–72.
24. Zbiciński I. Development and experimental verification of momentum, heat and mass transfer model in spray drying. *Chem Eng J Biochem Eng J*. 1995;58(2):123–133.
25. Fletcher DF, Guo B, Harvie DJE, Langrish TAG, Nijdam JJ, Williams J. What is important in the simulation of spray dryer performance and how do current CFD models perform? *Appl Math Model*. 2006;30(11):1281–1292.
26. Langrish TAG, Kockel TK. The assessment of a characteristic drying curve for milk powder for use in computational fluid dynamics modelling. *Chem Eng J* 2001;84:69–74.
27. Southwell DB, Langrish TAG, Fletcher DF. Use of computational fluid dynamics techniques to assess design alternatives for the plenum chamber of a small spray dryer. *Dry Technol*. 2001;19(2):257–268.
28. Langrish TAG. Multi-scale mathematical modelling of spray dryers. *J Food Eng*. 2009;93(2):218–228.
29. Aghbashlo M, Mobli H, Rafiee S, Madadlou A. An artificial neural network for predicting the physiochemical properties of fish oil microcapsules obtained by spray drying. *Food Sci Biotechnol*. 2013; 22(3):677–685.
30. Keshani S, Daud WRW, Woo MW, Talib MZM, Chuah AL, Russly AR. Artificial neural network modeling of the deposition rate of lactose powder in spray dryers. *Dry Technol*. 2012;30(4):386–397.
31. Yang XF, Xiao J, Woo MW, Chen XD. Three-dimensional numerical investigation of a monodisperse droplet spray dryer: validation aspects and multi-physics exploration. *Dry Technol*. 2015;33:742–756.
32. Fletcher DF, Langrish TAG. Scale-adaptive simulation (SAS) modelling of a pilot-scale spray dryer. *Chem Eng Res Des*. 2009;87(10):1371–1378.
33. Mezhericher M, Levy A, Borde I. Probabilistic hard-sphere model of binary particle–particle interactions in multiphase flow of spray dryers. *Int J Multiphase Flow*. 2012;43:22–38.
34. Lin SXQ, Chen XD. Changes in milk droplet diameter during drying under constant drying conditions investigated using the glass filament method. *Food Bioprod Process*. 2004;82(C3):213–218.
35. Oldfield DJ, Taylor MW, Singh H. Effect of preheating and other process parameters on whey protein reactions during skim milk powder manufacture. *Int Dairy J*. 2005;15(5):501–511.
36. Tatumi K, Kil JP. Influence of air parameters on spray drying energy consumption. *Revista Brasileira de Produtos Agroindustriais, Campina Grande*. 2010;12(1):45–54.
37. Ebrahimi A, Langrish TAG. Effect of humidity on in-process crystallization of lactose during spray drying. *Int J Chem Nucl Mater Metal Eng*. 2014;8(10):1030–1033.
38. Ståhl K, Claesson M, Lilliehorn P, Lindén H, Kjell B. The effect of process variables on the degradation and physical properties of spray dried insulin intended for inhalation. *Int J Pharm*. 2002;233:227–237.
39. Tonon RV, Brabet C, Hubinger MD. Influence of process conditions on the physicochemical properties of açai (Euterpe oleraceae Mart.) powder produced by spray drying. *J Food Eng*. 2008;88(3): 411–418.
40. Chen XD, Xie GZ. Fingerprints of the drying behaviour of particulate or thin layer food materials established using a reaction engineering model. *Food Bioprod Process*. 1997;75(4):213–222.
41. Chen XD, Lin SXQ. Air drying of milk droplet under constant and time-dependent conditions. *AIChE J*. 2005;51(6):1790–1799.
42. Patel KC, Chen XD, Lin SXQ, Adhikari B. A composite reaction engineering approach to drying of aqueous droplets containing sucrose, maltodextrin (DE6) and their mixtures. *AIChE J*. 2009; 55(1):217–231.
43. Nevers ND. *Physical and Chemical Equilibrium for Chemical Engineers*. New York: Wiley, 2002.
44. Lin SXQ, Chen XD, Pearce DL. Desorption isotherm of milk powders at elevated temperatures and over a wide range of relative humidity. *J Food Eng*. 2005;68(2):257–264.

Appendix: Reaction Engineering Approach

In this work, the kinetics of drying of droplets in spray dryer has been represented using the reaction engineering approach (REA). First introduced by Chen and Xie[40] and later modified by Chen and Lin,[41] REA was developed based on careful experimentation on the drying of milk droplets. The REA model assumes that evaporation is an activation process having to overcome an "energy barrier."[40] It follows that the rate of water evaporation or drying flux can be estimated from

$$-\frac{dm_w}{dt} = -m_s \frac{dX}{dt} \tag{A1}$$

$$= h_m A_p \left[\rho_{v,\mathrm{sat}} \exp\left(-\frac{\Delta E_v}{R_g T_p} \right) - \rho_{v,b} \right] \tag{A2}$$

Simplification of Eqs. A1 and A2 becomes

$$\frac{dm_w}{dt} = -h_m A_p \left(\rho_{v,s} - \rho_{v,b} \right) \tag{A3}$$

where m_w and m_s represent the mass of water and solids in a droplet (kg), X is the droplet average moisture content (kg water. kg^{-1}, on dry basis), $\rho_{v,\mathrm{sat}}$ and $\rho_{v,b}$ are saturated vapor concentration corresponding to average droplet temperature T_p and vapor concentration of bulk drying gas (kg m^{-3}) respectively, and $\rho_{v,s}$ is the surface vapor concentration (kg m^{-3}).

The dependence of activation energy (ΔE_v) on the average moisture content on dry basis can be normalized to define a dimensionless parameter called "relative activation energy" ($\Delta E_v / \Delta E_{v,b}$) given as

$$\frac{\Delta E_v}{\Delta E_{v,b}} = f(X - X_b) \tag{A4}$$

$\Delta E_{v,b}$ is equilibrium activation energy (the maximum possible activation energy), which is a function of bulk air temperature and humidity[40,41] and, X_b is the moisture content in equilibrium with the drying air condition.

The relative activation energy defined in Eq. A4 has been seen to be the indication of the degree of difficulty in removing water from the product.[42] Prior to drying, the droplet surface may be saturated with free water (i.e., at a high X value) and the difficulty to remove free moisture (relative activation

energy) is very low (close to zero or zero). The relative activation energy gradually increases when the droplet's moisture content is reduced during drying. When the moisture content approaches X_b, the relative activation energy is expected to be close to unity. The relationship between X and ΔE_v must be determined by experiments for different drying materials.

According to Chen and Lin, $f(X-X_b)$ may be expressed as

$$\frac{\Delta E_v}{\Delta E_{v,b}} = a.e^{\left(-b(X-X_b)^d\right)} \tag{A5}$$

where a=0.998, b=1.405, and d=0.930 for skim milk of 20wt %.[41]

Correlations used in skim milk drying ode model

Linear shrinkage was assumed and the diameter of the particle was calculated based on Lin and Chen empirical model as follows

$$d_{p,t_e} = d_{p,0}\left[\beta + (1-\beta)\frac{X}{X_0}\right] \tag{A6}$$

where $d_{p,te}$ and $d_{p,0}$ represent the droplet diameter at time t_e and zero respectively, β=0.59 for 20wt % skim milk droplet.

The rate of number of particles at each elevation in the chamber is a constant value due to the plug flow assumption

$$\theta = \frac{\dot{m}_{p,\text{total}} \Big/ \rho_{p,\text{wet}}}{\frac{4}{3}\pi\left(\frac{d_{p,0}}{2}\right)^3} \tag{A7}$$

Density of the wet bulk air was calculated based on an ideal gas assumption

$$\rho_b = \frac{PMr_{\text{equivalent}}}{R_g T_b} \tag{A8}$$

The equivalent molecular weight ($Mr_{\text{equivalent}}$) was computed by mass weighting between the molecular weight of water and air

$$Mr_{\text{equivalent}} = \frac{1}{\frac{x_{\text{water}}}{Mr_{\text{water}}} + \frac{x_{\text{air}}}{Mr_{\text{air}}}} \tag{A9}$$

Defining the mass fraction of water and air as the following

$$x_{\text{water}} = \frac{Y}{Y+1} \tag{A10}$$

$$x_{\text{air}} = \frac{1}{Y+1} \tag{A11}$$

On rearrangement

$$Mr_{\text{equivalent}} = \frac{Mr_{\text{air}}\,(Y+1)}{\left(\frac{Mr_{\text{air}}\,Y}{Mr_{\text{water}}}+1\right)} \tag{A12}$$

Putting this equation back into the original equation and taking Mr_{air}=29, Mr_{water}=18, P=101324

$$\rho_b = \left(\frac{353.15}{T_b}\right)\left(\frac{Y+1}{1.61Y+1}\right) \tag{A13}$$

The saturated vapor pressure was calculated from Nevers (2002)[43]

$$P_{\text{sat}} = \left(\frac{101325}{760}\right).10\left(7.94917 - \frac{1657.462}{T+227.02}\right) \tag{A14}$$

In applying Eq. A14, the temperature T is expressed in °C. With surface saturated vapor density and ambient vapor density calculated from

$$\rho_{v,\text{sat}} = \frac{P_{\text{sat}} Mr_{\text{water}}}{R_g T_p} \tag{A15}$$

$$\rho_{v,b} = \frac{P_{\text{sat}} Mr_{\text{water}}}{R_g T_b} \tag{A16}$$

The equilibrium moisture was taken from the work of Lin et al. (2005)[44] following the GAB equation,

$$X_b = \frac{CK(0.06156)}{(1-Ka_w)(1-Ka_w+Ca_w)} \tag{A17}$$

in which the two temperature dependent constants take the Arrhenius form

$$C = 0.001645\exp\left(\frac{24831}{R_g T_b}\right) \tag{A18}$$

$$K = 5.17\exp\left(\frac{-5118}{R_g T_b}\right) \tag{A19}$$

a_w is water activity expressed as $\rho_{v,b}/\rho_{v,\text{sat}}(T_b)$, m_0 is monolayer moisture content set to 0.06156.

Manuscript received Feb. 8, 2015, and revision received June 1, 2015.